Tumor-specific MHC-II expression drives a unique pattern of resistance to immunotherapy via LAG-3/FCRL6 engagement

Douglas B. Johnson,[1] Mellissa J. Nixon,[1] Yu Wang,[2] Daniel Y. Wang,[1] Emily Castellanos,[1] Monica V. Estrada,[3] Paula I. Ericsson-Gonzalez,[4,5] Candace H. Cote,[1] Roberto Salgado,[6,7] Violeta Sanchez,[4] Phillip T. Dean,[1] Susan R. Opalenik,[1] Daniel M. Schreeder,[8] David L. Rimm,[9] Ju Young Kim,[10] Jennifer Bordeaux,[10] Sherene Loi,[7] Leora Horn,[1] Melinda E. Sanders,[4,5] P. Brent Ferrell Jr.,[1] Yaomin Xu,[2] Jeffrey A. Sosman,[11] Randall S. Davis,[12] and Justin M. Balko[1,5]

[1]Department of Medicine and [2]Department of Biostatistics, Vanderbilt University Medical Center, Nashville, Tennessee, USA. [3]Department of Pathology, University of California, San Diego, San Diego, California, USA. [4]Department of Pathology Microbiology, and Immunology, and [5]Breast Cancer Research Program, Vanderbilt University Medical Center, Nashville, Tennessee, USA. [6]Department of Pathology, GZA-ZNA Hospitals, Antwerp, Belgium. [7]Department of Oncology, University of Melbourne and Peter MacCallum Cancer Centre, Melbourne, Victoria, Australia. [8]Clearview Cancer Institute, Huntsville, Alabama, USA. [9]Departments of Pathology and Medicine, Yale University, New Haven, Connecticut, USA. [10]Navigate BioPharma Services Inc., a Novartis Company, Carlsbad, California, USA. [11]Department of Medicine, Northwestern University, Chicago, Illinois, USA. [12]Departments of Medicine, Microbiology, and Biochemistry and Molecular Genetics, University of Alabama, Birmingham, Alabama, USA.

Immunotherapies targeting the PD-1 pathway produce durable responses in many cancers, but the tumor-intrinsic factors governing response and resistance are largely unknown. MHC-II expression on tumor cells can predict response to anti–PD-1 therapy. We therefore sought to determine how MHC-II expression by tumor cells promotes PD-1 dependency. Using transcriptional profiling of anti–PD-1–treated patients, we identified unique patterns of immune activation in MHC-II+ tumors. In patients and preclinical models, MHC-II+ tumors recruited CD4+ T cells and developed dependency on PD-1 as well as Lag-3 (an MHC-II inhibitory receptor), which was upregulated in MHC-II+ tumors at acquired resistance to anti–PD-1. Finally, we identify enhanced expression of FCRL6, another MHC-II receptor expressed on NK and T cells, in the microenvironment of MHC-II+ tumors. We ascribe this to what we believe to be a novel inhibitory function of FCRL6 engagement, identifying it as an immunotherapy target. These data suggest a MHC-II–mediated context-dependent mechanism of adaptive resistance to PD-1-targeting immunotherapy.

Introduction

Immune checkpoint inhibitors that block the interaction between programmed death-1 (PD-1) and its ligand (PD-L1) have transformed the treatment landscape of numerous solid tumors (1). These agents unleash restrained preexisting antitumor immune responses, leading to durable disease control in a substantial fraction of treated patients. Despite these advances, intrinsic and acquired resistance curtails clinical benefits in most patients.

Molecular drivers of therapeutic resistance are incompletely characterized. Described resistance mechanisms include downregulation of antigen machinery by somatic mutations in JAK/STAT pathways (2, 3), alternative immune checkpoint expression (4), loss or lack of immunogenic neoantigens (5–10), and tumor-intrinsic gene expression programs involving angiogenesis and wound healing (11). Identifying effective therapeutic strategies to overcome mechanisms of resistance and characterizing novel drivers remain critical unmet needs.

We have previously shown that MHC-II expression on tumor cells represents an autonomous phenotype that is associated with enhanced response to PD-1–targeted immunotherapy (12), a finding subsequently validated in other tumor types (13) and with combination immunotherapy (14). While MHC-II expression is not

required for response to immunotherapy in melanoma, tumors demonstrating this phenotype have particularly frequent and profound clinical responses (12). Herein, through dedicated immunohistological and RNA-sequencing analyses of MHC-II phenotypes in tumors, we identified patterns of inflammation present in those expressing MHC-II. MHC-II expression on tumor cells promotes antitumor immunity and facilitates the recruitment of CD4+ T cells, which corresponds to increased expression of CXCR3-binding T cell–recruiting cytokines. As tumors adapt to this microenvironment, either during cancer progression or during treatment with immunotherapies targeting the PD-1/L1 axis, we demonstrate that they acquire immunosuppressive signals through alternative checkpoints that antagonize MHC-II expression, such as LAG-3.

Finally, we show that another MHC-II receptor, Fc receptor–like 6 (FCRL6), is present in the tumor microenvironment of MHC-II+ tumors and is subsequently upregulated following progression on PD-1–directed immunotherapy. We demonstrate evidence that, similar to Lag-3, FCRL6 provides an immunosuppressive signal that directly represses NK cell cytotoxic activity and effector T cell cytokine secretion when it engages MHC-II. Therefore, we identify FCRL6 as a checkpoint and immunotherapy target. Collectively, these data suggest a mechanism whereby an intrinsic tumor phenotype drives a unique pattern of adaptive resistance to immunotherapy.

Results

MHC-II+ tumors are enriched with gene expression patterns of adaptive immunity. We have previously shown that melanomas with constitutive tumor cell–autonomous MHC-II/HLA-DR expression are associated with high CD4 and CD8 infiltration and enhanced responses to PD-1–targeted immunotherapy (12, 15), a finding subsequently confirmed by others (14). Furthermore, MHC-II+ melanoma cell lines (grown in the absence of stroma or IFN-γ–expressing cells) demonstrate intrinsic gene expression patterns of inflammation and autoimmunity (12). However, HLA-DR expression by melanoma cells in vivo could be due to membrane exchange (trogocytosis) in an inflammatory milieu (16). To confirm that HLA-DR is endogenously expressed by tumor cells, we performed dual RNA–in situ/IHC analysis for CIITA and HLA-DR, respectively, on melanoma specimens. As shown in Supplemental Figure 1 (supplemental material available online with this article; https://doi.org/10.1172/jci.insight.120360DS1), MHC-II/HLA-DR+ tumor cells expressed mRNA for CIITA, the master regulator of MHC-II gene transcription, suggesting this is a tumor cell–autonomous phenotype in human melanoma.

To extend upon our previously published data, we performed RNA-sequencing analysis on a series of anti–PD-1–treated melanoma and non–small cell lung cancers (n = 58, including 50 pre–anti–PD-1 samples and 8 samples obtained after anti–PD-1 following acquired resistance) and scored tumor-specific HLA-DR expression by IHC (HLA-DR staining available on 41 of 58; Figure 1A) prior to their treatment with PD-1–targeted immunotherapy. Tumors with at least 5% of tumor cells expressing cell-surface HLA-DR demonstrated similar gene set enrichment as observed in our previously published analyses of melanoma cell lines (12). The gene sets enriched (FDR < 5%) in HLA-DR+ tumors included those associated with allograft rejection, viral myocarditis, autoinflammatory disease (asthma), and IFN-γ response pathways (Figure 1B). Although HLA-DR is an IFN-γ–inducible gene, our previous studies performed on cultured tumor cell lines (without IFN-γ) suggested that this finding is likely linked, at least partially, to the intrinsic state of the tumor cells, rather than a direct measure of IFN-γ activity in the microenvironment. This is supported by a high degree of overlap between enriched gene sets in MHC-II+ human tumors and cultured cell lines (in the absence of IFN-γ) identified in this study and our previous work (12) (Figure 1C). HLA-DR+ tumors had greater mRNA expression of MHC-II genes, such as *HLA-DRA*, although the association was weak, reflecting the independent contribution of HLA-DR+ stroma (e.g., macrophages, dendritic cells) to this measurement. In addition, consistent with our prior IHC observations, HLA-DR+ tumors had higher *CD8A* and *CD4* expression, without enhanced regulatory T cell markers, such as *Foxp3* (Supplemental Figure 2).

MHC-II+ tumors are associated with higher expression of immune checkpoint receptors. To explore the effects of tumor cell–autonomous MHC-II expression on antigen presentation machinery and immune checkpoints, we correlated HLA-DR expression (scored by IHC) with genes associated with MHC-II (*HLA-DRA*), MHC-I (*HLA-A*), T cell repression (*PD-1/PDCD1*, *PD-L1/CD274*, *IDO1*, *TIM-3/HAVCR2*, and *LAG3*), T cell activation (*IFNG*), monocyte infiltration (CD68), and a ubiquitous marker (*TP53*) as a control (Figure 1D). The expression of most immune-related genes were positively correlated with one another. HLA-DR IHC expression, as scored only in the tumor compartment, also correlated with most immune genes, but less strongly with the myeloid marker *CD68*. Interestingly, all examined immune checkpoint receptor genes
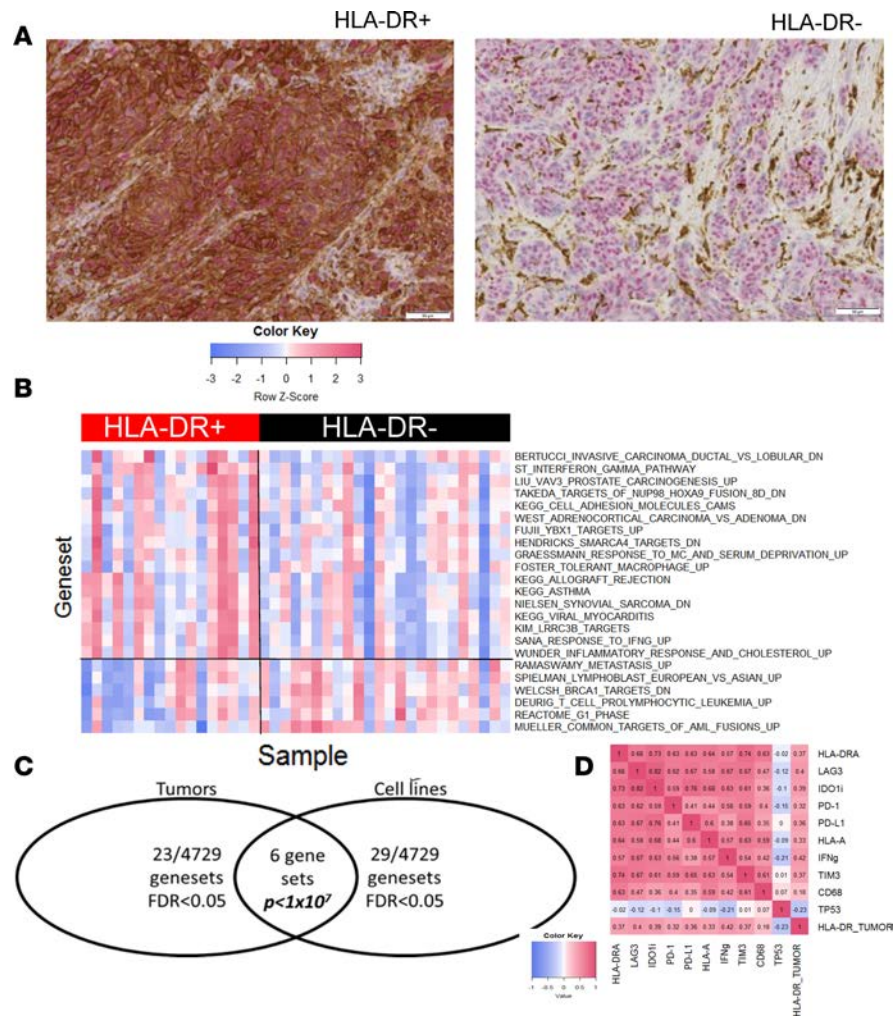
Figure 1. MHC-II/HLA-DR expression in patient tumor samples is associated with unique patterns of inflammation and enhanced CD4, CD8, and LAG-3^{+} infiltrate. (**A**) Representative images of IHC from HLA-DR[+] and HLA-DR[−] tumors. HLA-DR is stained in brown (DAB), and Sox10, a nuclear melanoma marker, is stained in pink (Mach Red). Scale bar: 50 μm. (**B**) Gene set analysis from RNA-sequencing analysis of IHC-defined tumor HLA-DR[+] (≥5% tumor cells) or HLA-DR[−] (<5% tumor cells) melanoma and lung specimens. After significant (FDR < 10%) gene set scores were defined, scores were created as the mean of all genes in each signature for each sample and plotted as row-standardized Z-scores with heatmap representation. (**C**) Overlap of enriched gene sets in MHC-II[+] tumors versus melanoma cell lines (ref. 12). (**D**) Pearson's correlation matrix of gene expression associations between immune response and inhibitory markers among PD-1–treated patient samples from melanoma and lung cancer (n = 50). Data represent correlation among TPM RNA-sequencing values, except "HLA-DR_TUMOR," which is the correlation with tumor HLA-DR percent positivity by IHC (n = 41 of 50 available data points). Values in the individual boxes represent the Pearson's correlation coefficient.

also highly correlated with HLA-DR positivity, and the most significant of these was *LAG3*. These associations were also evident when stratifying tumors by MHC-II[+] ≥5% (Figure 2A). Of particular interest in this analysis was the association of HLA-DR tumor cell positivity with *LAG3*, which competes with CD4 as a ligand for MHC-II, thereby suppressing MHC-II–mediated antigen presentation (17, 18).

To determine what cell types in the melanoma microenvironment express LAG-3, we performed mass cytometry (CyTOF) on two human patient melanoma resections as well as PBMCs from a healthy individual. viSNE analyses of resected melanomas demonstrated the following observations (Supplemental Figure 3A). LAG-3 was exclusively expressed by T cells, primarily CD8^{+} T cells, but much less so by CD4^{+} cells. LAG-3^{+} cells were a less abundant subset of PD-1^{+} T cells, which were found primarily on both CD4^{+} and CD8^{+} antigen-experienced (CD45RO^{+}) and effector (TBET^{+}) cells in the tumor microenvironment. A subset of PD-1^{+} cells was also Ki67^{+} (cycling). However, LAG-3 appeared to be exclusive of Ki67 positivity,
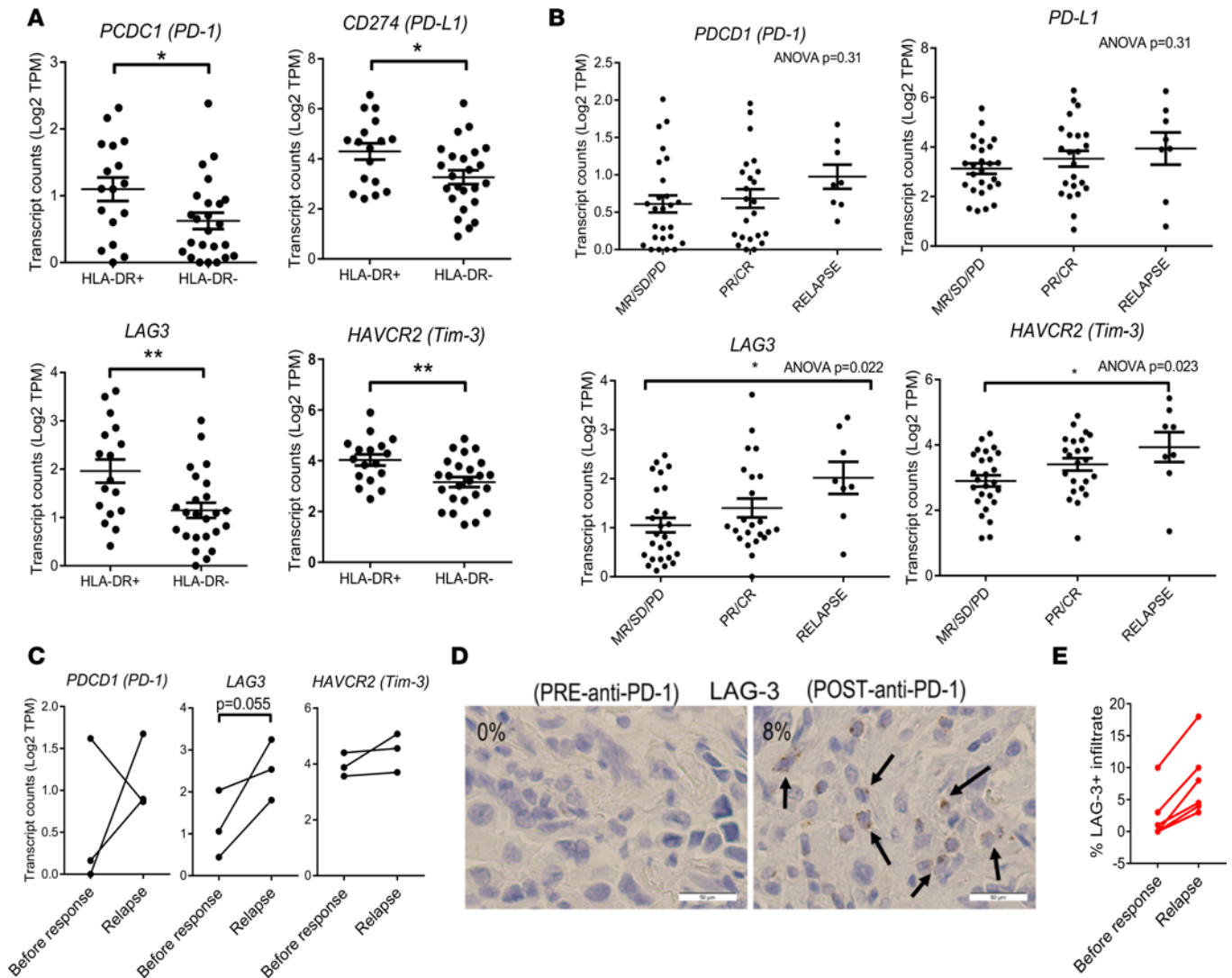
Figure 2. MHC-II/HLA-DR expression in patient tumor samples is associated with LAG-3+ infiltrate. (**A**) RNA-sequencing expression levels of checkpoint and checkpoint ligands by HLA-DR status of the tumor. *n* = 41; *P < 0.05; **P < 0.01, 2-tailed *t* test. (**B**) RNA-sequencing expression levels of checkpoint and checkpoint ligands by patient immune-related response criteria. PD, progressive disease; SD/MR, stable disease or mixed response; PR, partial response; CR, complete response; RELAPSE, sample collected at relapse/progression after initial PR/CR. *n* = 57; *P < 0.05, Tukey's post hoc test. (**C**) RNA-sequencing expression levels of checkpoints in 3 pairs of matched prerespose and postrelapse specimens. *P* value represents paired 2-tailed *t* test. (**D**) Representative IHC for LAG-3 in a melanoma sample before anti–PD-1 response and at progression. Scale bar: 50 μm. (**E**) IHC analysis for LAG-3+ TILs in 6 paired melanoma specimens before anti–PD-1 response and at progression.

possibly reflecting a more senescent phenotype. LAG-3 was not detected on CD25+CD4+ cells, suggesting its dissociation from a classical T regulatory phenotype. Interestingly, although neither tumor expressed abundant MHC-II (HLA-DR), MHC-II was highly expressed by B cells and a substantial fraction of PD-1+ T cells that also appeared to overlap with LAG-3 expression (Supplemental Figure 3B).

Next, we examined the association between gene expression of checkpoint molecules and ligands with annotated clinical response to anti–PD-1 in these patients. Included in this analysis were 49 pretreatment tumors as well as tumor samples available from patients who initially responded to anti–PD-1 therapy but subsequently progressed (i.e., relapsed) (*n* = 6 patients and *n* = 8 samples, with 3 isolated resections/biopsies from a single patient). When comparing treatment response groups, *LAG3* and *HAVCR2* (encoding Tim-3) showed differential expression by ANOVA. Of interest, neither *LAG3* nor *HAVCR2* expression obviously correlated with intrinsic resistance (in responding vs. nonresponding patients), but they were significantly higher in progression (relapse) specimens (i.e., acquired resistance) (Figure 2B). *IFNG* expression was also higher in relapsed patients. Although an IFN-γ–response signature was not

elevated, it showed a similar trend, suggesting that the majority of these tumors had not lost IFN-γ activity or expression (Supplemental Figure 4). Neither transcript expression of MHC-I (HLA-A) nor MHC-II (HLA-DRA) was associated with clinical responses to PD-1 in patients, stressing the unique information gained by examining MHC-II protein expression by IHC specifically in tumor cells (12) (Supplemental Figure 5). Finally, our cohort included 3 patients in whom paired tumor samples were available both prior to response to anti–PD-1 and at relapse/progression. We hypothesized that alternative checkpoints (LAG-3 and HAVCR2) would be upregulated in matched samples after progression on PD-1. When considering checkpoint molecule expression (*PDCD1*, *LAG3*, and *HAVCR2*) in these 3 matched pairs, both *LAG3* and *HAVCR2* demonstrated a trend toward enrichment in 3 of 3 specimens (1-tailed *t* test *P* = 0.15), although enrichment of *LAG3* was more striking (1-tailed *t* test *P* = 0.055; Figure 2C). IHC analysis for LAG-3+ tumor-infiltrating lymphocytes (TILs) confirmed this trend (*n* = 5 pairs, before and at acquired resistance, all unique patients; Figure 2, D and E). Upon resistance to anti–PD-1, increased *LAG3* and *HAVCR2* have been observed in both humanized murine models (19) and patients (4).

Association of MHC-II expression with inflammation and LAG-3 expression in breast cancer. We previously identified tumor cell–autonomous MHC-II expression as an important biomarker in breast cancer. MHC-II+ breast tumors were found to have a greater degree of TILs after neoadjuvant chemotherapy, which correlates with improved outcomes after surgical resection (20). Since we have previously molecularly characterized this series of 112 triple-negative breast cancers (TNBCs) for MHC-II/HLA-DR expression in the tumor compartment (20), we asked whether a similar association of MHC-II+ tumors with LAG-3+ TILs (Figure 3, A and B) could be observed in this cohort. HLA-DR was scored using automated quantitative analysis (AQUA; Figure 3C). We found a strong association of the presence of LAG-3+ TILs in tumors with high HLA-DR expression, both across the entire series and after controlling for the intrinsically higher rate of TILs in HLA-DR+ tumors by including only heavily infiltrated (TILs >20%) tumors in the analysis (Figure 3D and Supplemental Figure 6). Consistent with our findings in melanoma (12), HLA-DR+ tumors were also strongly associated with the presence of CD4 and, to a lesser degree, CD8 infiltrates. However, the enrichment for CD4+ T cells in the HLA-DR+ tumors was significantly higher (*P* < 0.01) (Figure 3E). HLA-DR positivity also correlated with higher PD-L1 expression in the tumor-associated stroma, but the association of PD-L1+ stroma with LAG-3+ TILs was weaker than that of HLA-DR, suggesting that HLA-DR positivity is associated with LAG-3+ TILs and higher PD-L1 expression in the tumor microenvironment and that LAG-3 positivity and PD-L1 positivity are not necessarily directly correlated (Figure 3F and Supplemental Figure 6B).

Enforced expression of MHC-II promotes tumor rejection, CD4+ T cell recruitment, and a specific pathway to immune evasion. To better understand the direct role of MHC-II expression on the tumor microenvironment, we enforced expression of MHC-II on MMTV-neu breast tumor cells through transduction of *Ciita*, the master regulator of MHC-II. Cells transduced with *Ciita* were strongly IA-IE+ (murine MHC-II), by flow cytometry analysis (Figure 4A). When equivalent CIITA+ or vector control cells were injected orthotopically into the mammary fat pads of wild-type *FVB/n* mice, a substantially greater rejection rate was observed (Figure 4, B and C). Rejecting mice were 100% resistant to rechallenge (data not shown). In mice that did form tumors, the tumor growth rate was similar in both MHC-II+ and MHC-II− tumors (Supplemental Figure 7), suggesting a robust adaptive resistance to the presence of tumor-autonomous MHC-II in a subset of tumors.

Enforced expression of MHC-II has been shown to result in increased antitumor inflammation, Th1 differentiation, and antigen-specific CD4+ T cells (21–24). Consistent with this, we found that tumors that did form in the presence of enforced MHC-II had greater fractions of CD4+ T cells (normalized to total TILs), with no change in the regulatory compartment (Foxp3+) (Figure 4D). CD8+ T cells showed a downward trend when normalized to total TILs; however, this was reflective of the increased percentage of CD4+ T cells, and absolute extent of CD8+ T cell infiltrate was not affected by MHC-II status. Gene expression analysis of refractory (those tumors evading initial immunologic rejection) MHC-II+ and control MMTV-neu tumors showed enhanced expression *Ciita*-regulated genes (suggesting MHC-II expression was not lost in these tumors) (Figure 5A and Supplemental Figure 8). In addition, both *Pdcd1/Pd-1* and *Lag3* were more highly expressed in MHC-II+ tumors. *Havcr2/Tim-3* was not highly expressed or enriched in MHC-II+ tumors (Figure 5B). Collectively, these data suggest that MHC-II expression in tumor cells promotes an antitumor immune environment coinciding with recruitment of CD4+ T cells and the eventual engagement of Pd-1 and Lag3 to suppress antitumor immunity.
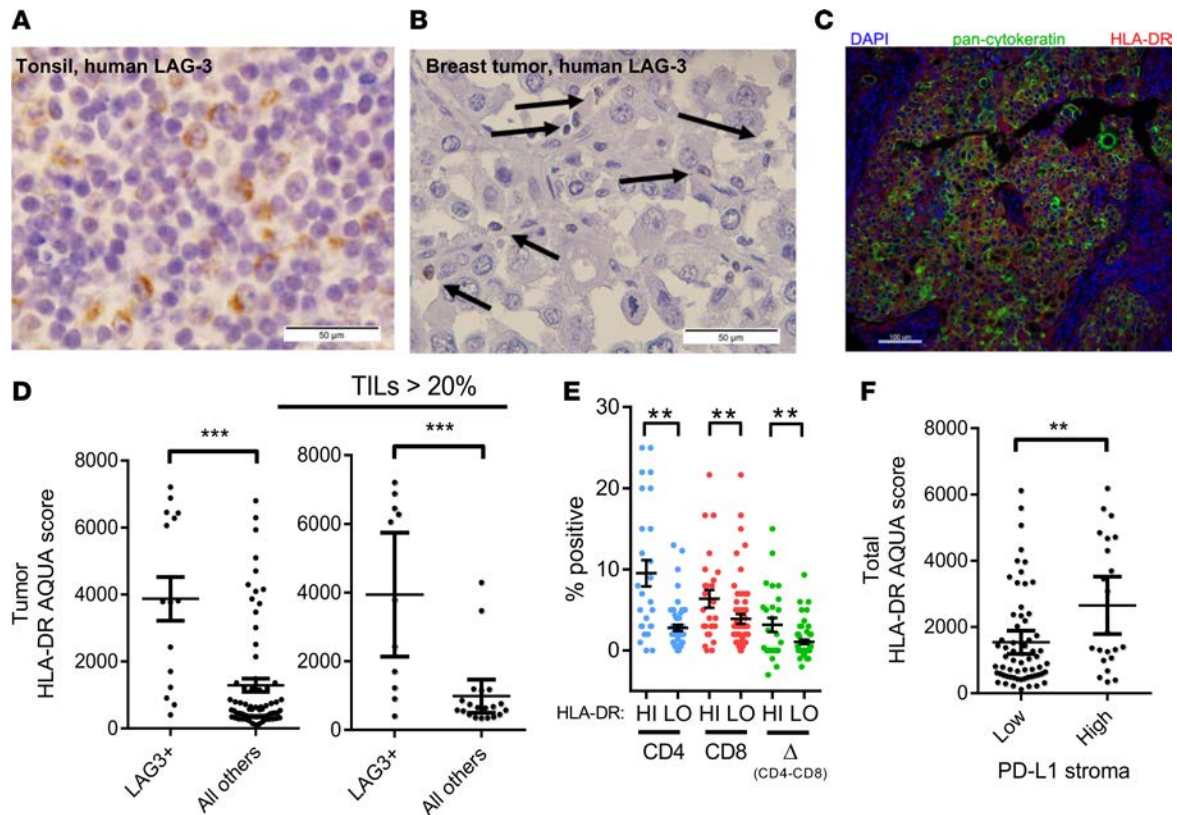
Figure 3. MHC-II+ breast tumors recruit CD4+ T cells and are associated with Lag-3+ TILs. (**A**) Representative positive control for Lag-3 IHC in human tonsil. Scale bar: 50 μm. (**B**) Representative Lag-3+ breast cancer TILs by IHC. Arrows indicate Lag-3+ TILs. Scale bar: 50 μm. (**C**) Representative AQUA immunofluorescence image of a HLA-DR+ breast tumor case. Scale bar: 100 μm. (**D**) Difference in tumor-specific HLA-DR expression among LAG-3+ and LAG-3− infiltrated triple-negative breast cancers in all patients ($n = 86$; left) and only those patients with a percentage of stromal TILs >20% ($n = 31$; right). ***$P < 0.001$, 2-tailed t test. (**E**) CD4 and CD8 and the difference between CD4 and CD8 infiltration in HLA-DR–high (HI) and HLA-DR–low (LO) expressing tumors. **$P < 0.01$, 2-tailed t test. (**F**) Association of stromal (noncytokeratin+) PD-L1 expression with HLA-DR expression. **$P < 0.01$, 2-tailed t test.

MHC-II expression promotes the expression of T cell–recruiting chemokines. The mechanism behind recruitment of T cells to the immune microenvironment of MHC-II+ tumors is unclear. However, we noticed from our gene expression analyses that known T cell chemoattractant cytokines (e.g., *Cxcl13*, *Ccl5*) were elevated in MHC-II+ MMTV-neu tumors (Figure 5A). To determine if chemokine production was a direct byproduct of Ciita expression, we evaluated MMTV-neu cells grown ex vivo for expression of *Cxcl9*, *Cxcl10*, *Cxcl11*, *Cxcl13*, and *Ccl5*. We detected enhanced expression of these chemokines at the mRNA level, indicating they may be downstream of Ciita transcriptional activation (Figure 5C). Consistent with this hypothesis, large-scale ChIP-seq experiments have identified DNA binding of the CIITA/RFX5 complex at the promoter of *CXCL9* and *CXCL10* (25). Thus, the likely mechanism whereby CIITA expression mediates an enhanced inflammatory environment is via increased chemoattractant cytokines, which promote the recruitment of Th1 and cytotoxic T lymphocytes to the microenvironment, exacerbating inflammatory signals. Expression of each of these ligands was also confirmed in vivo (Figure 5D). However, eomesodermin (*Eomes*) expression was elevated as well in these tumors, suggesting the potential for effector T cell exhaustion (Supplemental Figure 9A).

Similar elevation of these markers was present in MHC-II+ melanomas (Figure 6A and Supplemental Figure 9B). A high degree of coexpression was also observed in primary breast cancers, supporting the interdependency of these markers in the MHC-II+ phenotype (Figure 6B). Cxcl9, Cxcl10, and Cxcl11 (and their human orthologs), which are chiefly produced by tissue-resident and endothelial cells, bind the Cxcr3 receptor on Th1 and cytotoxic T cells to license entry into sites of inflammation (26). Interestingly, increased *Cxcr3* expression was also detectable in the tumor microenvironment of Ciita+ MMTV-neu tumors (Supplemental Figure 10). In comparison, we did not observe substantial differential or absolute expression of myeloid chemokines, such as *Ccl2*, *Cxcl15* (IL-8), or *Il-6*, although there was a statistically significant increase in *Il-8* in Ciita+ tumors (Supplemental Figure 11).
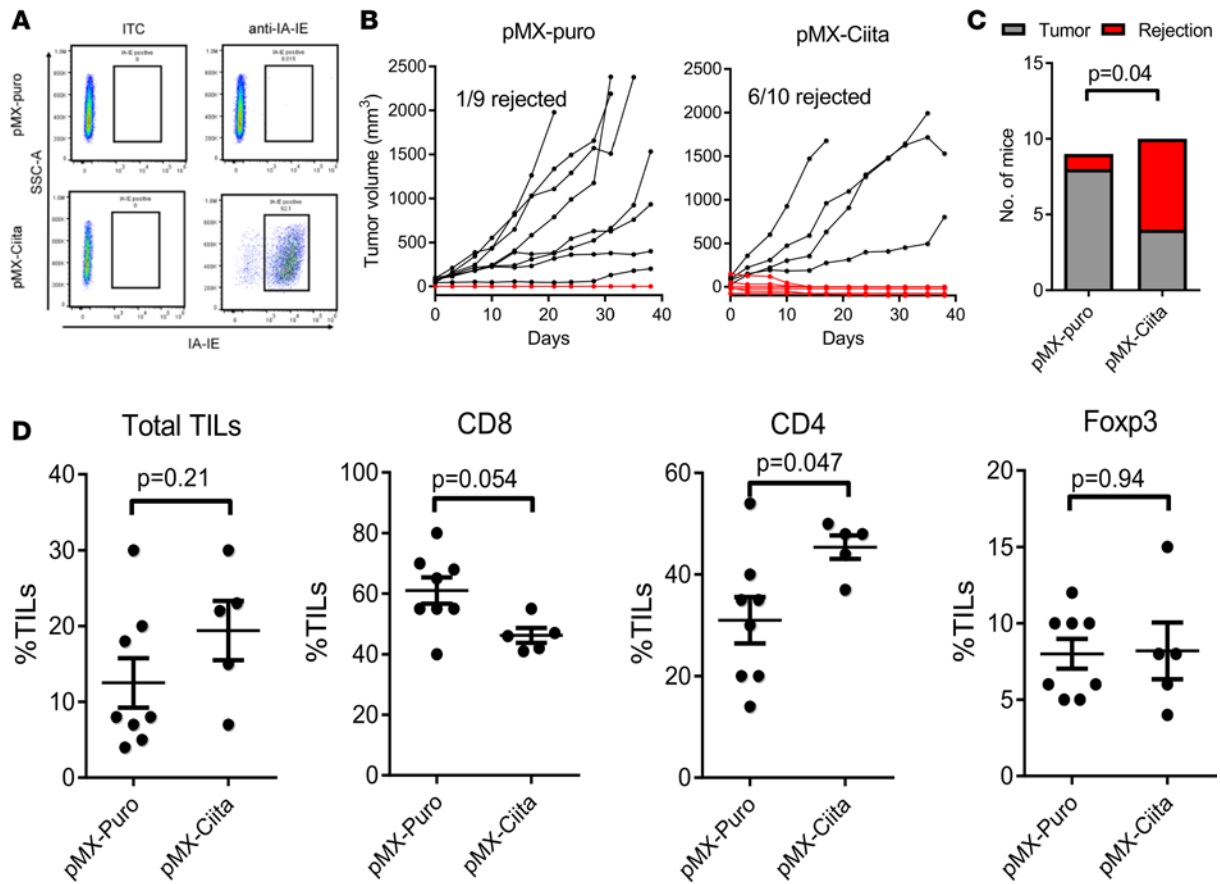
Figure 4. MHC-II expression in murine mammary carcinoma potentiates antitumor immunity. (**A**) Flow cytometry of MMTV-neu cells transduced with *Ciita* or vector control, stained with anti–MHC-II–Alexa Fluor 488 (IA-IE) or isotype control. (**B**) Tumor growth or orthotopic MMTV-neu cells in wild-type syngeneic *FVB/n* mice. Red lines represent rejected engraftments. (**C**) Proportions of rejected tumor engraftments for control or Ciita+ MMTV-neu cells. *P* value represents Fisher's exact test. (**D**) Tumors (*n* = 12) from **B** that were not rejected were examined by H&E for TILs and T cell compartments by IHC (CD8, CD4, and Foxp3) and scored as a percentage of total TILs. *P* values represent 2-tailed Mann-Whitney test.

A combination of PD-1 and Lag-3 immune checkpoint inhibitor therapy enhances antitumor immunity in MHC-II+ tumors. We next hypothesized that MHC-II+ tumors may generate direct dependence on PD-1 and Lag-3 in T cells, resulting in the generation of tumor tolerance to maintain immunologic equilibrium. To test this hypothesis, we utilized MMTV-neu tumor cells transduced to enforce expression of Ciita (or vector control), as above, according to the experimental design shown in Figure 7, A and B. Ten days after orthotopic implantation, mice were treated with anti-IgG (control), anti–PD-1, or the combination of anti–PD-1 and anti–Lag-3 for 2 weeks. Only mice with palpable and actively growing tumors at the start of therapy were treated in order to reduce confounders associated with enhanced immunogenicity and rejection observed in untreated Ciita+ tumors. A moderate treatment effect was observed in the combination arm in pMX-puro (control) tumors, but a pronounced antitumor effect was observed in the combination arm for Ciita+ tumors, with 6 of 8 mice exhibiting complete tumor rejection ($P < 0.05$, χ^2 test; Figure 7C). Flow cytometry analysis of lymphoid compartments demonstrated enhanced PD-1+/Lag-3+ CD4+ and CD8+ T cells in the proximal lymph node, with a similar trend observed in the spleen but not the contralateral lymph node (Figure 7D and Supplemental Figure 12). A similar effect was observed in tumor-infiltrating CD8 cells (Figure 7E). Thus, MHC-II positivity on tumor cells can elicit enhanced dependency on T cell checkpoints, including Lag-3, which can be overcome therapeutically.

Alternative MHC-II ligands are upregulated in MHC-II+ tumors and promote suppression of effector cell cytotoxicity. Given these findings, we hypothesized that other MHC-II receptors on lymphocytes may exist with similar functionality to Lag-3. FCRL6 is an immunoreceptor that is structurally related to classical Ig-binding leukocyte Fc receptors but was also shown to be a ligand for MHC-II (27). FCRL6 is an ITIM-bearing Ig superfamily member expressed by cytotoxic NK cells and effector memory CD8+ T cells (28, 29). Thus, we hypothesized that FCRL6 may function as a novel immune checkpoint to sup-
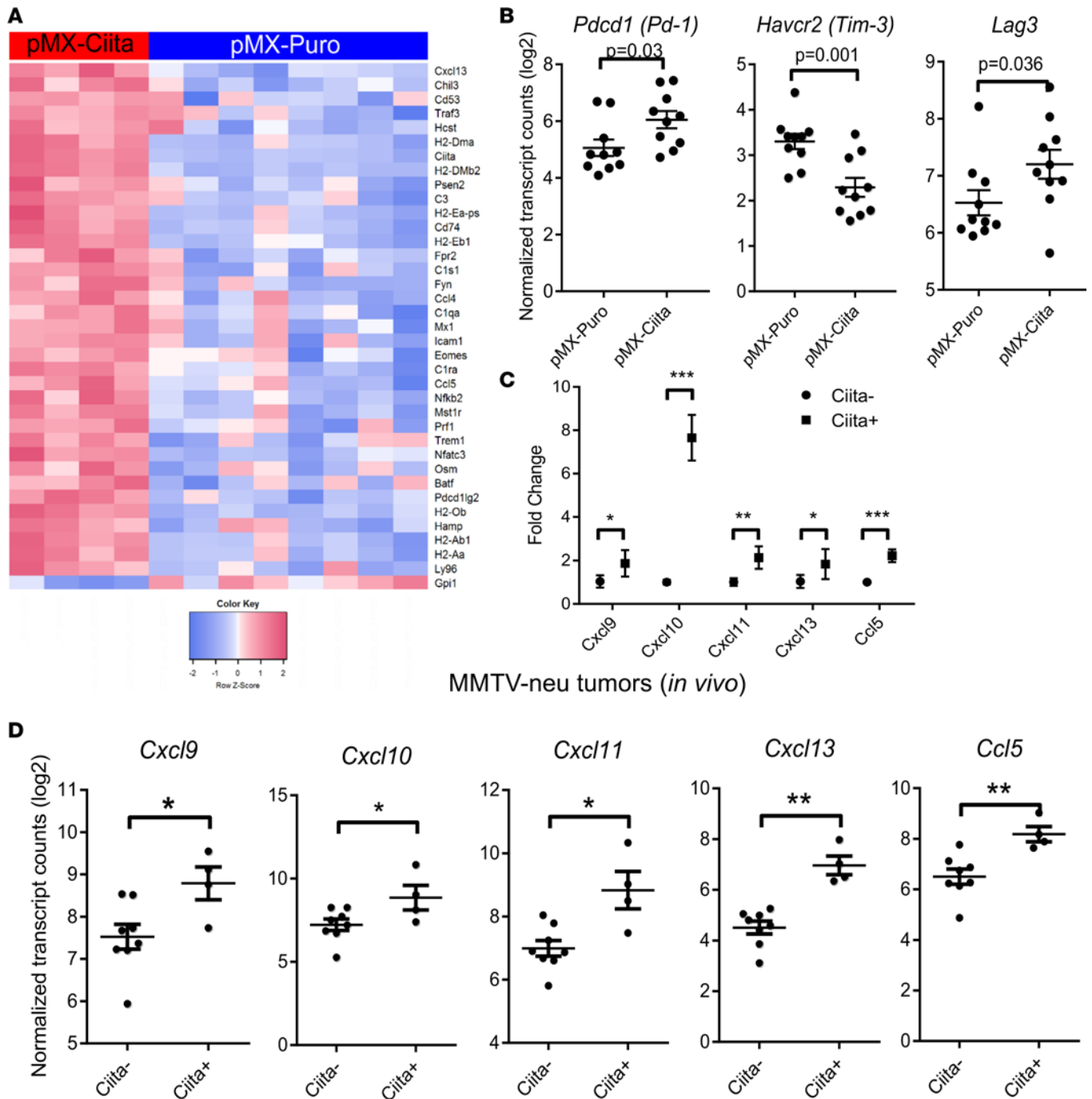
Figure 5. Enhanced T cell–recruiting chemokines and Lag3 expression in MHC-II⁺ murine tumors. (A) Heatmap visualization of altered gene expression levels in nonrejected tumors from Figure 2H. Transcript counts (NanoString PanCancer Immune profiling) were row normalized/standardized for visualization. **(B)** Gene expression levels of immune checkpoints Pd-1, Tim-3, and Lag-3 in Ciita⁺ and control tumors (n = 20). **(C)** Cultured MMTV-neu tumor cells (cell line) expressing Ciita or vector control were analyzed by quantitative real-time PCR for tumor-specific changes in T cell–recruiting chemokines. n = 3 independent experiments. *P < 0.05; **P < 0.01; ***P < 0.001, a 2-tailed t test. **(D)** NanoString gene expression data from MMTV-neu Ciita⁺ or vector control tumors (n = 12) harvested at humane endpoints (1.5–2 cm³) were queried for expression levels of T cell–attracting chemokines (see Supplemental Figure 9A fore eomesodermin [*Eomes*]). *P < 0.05; **P < 0.01, 2-tailed t test.

press effector cell activity when engaged with MHC-II. The regulation of NK cell cytotoxicity by MHC class I molecules has been well characterized, but evidence also exists that MHC class II expression can protect target cells from NK cell–mediated killing. Enforced expression of HLA-DR by K562 cells, a classic human erythroleukemic MHC-II–negative target cell line, was found to inhibit lysis by freshly isolated human NK cells in vitro (30). Furthermore, transplantation of K562 cells into NOD/SCID
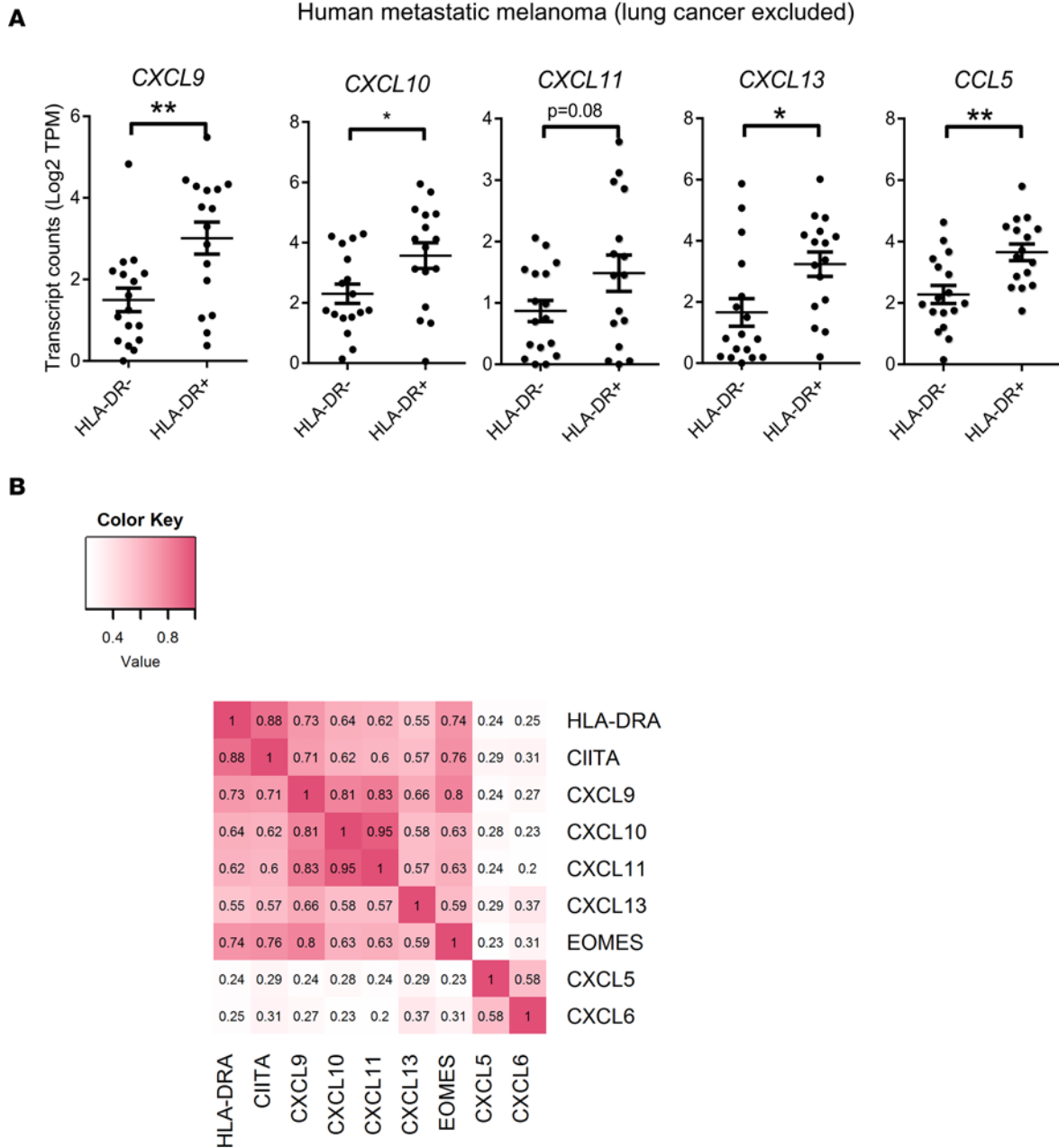
Figure 6. Enhanced T cell–recruiting chemokines in MHC-II+ human tumors. (**A**) RNA-sequencing gene expression data from HLA-DR+ and HLA-DR− tumors (*n* = 41) were analyzed for differences in the human orthologs for chemokines in Figure 5. *P < 0.05, **P < 0.01, by Mann Whitney U test. (**B**) TCGA breast cancer data set was utilized to explore correlations between HLA-DRA mRNA and T cell chemokines across over 1000 patients. A correlation matrix was generated showing the Pearson's correlation coefficient across each gene pair.

mice followed by adoptive transfer of human PBMCs demonstrated that K562 tumors expressing HLA-DR were dramatically protected from elimination by human NK cells in vivo (31).

Because FCRL6 is downregulated upon exposure to IL-2 or IL-15 (28), using expanded primary human NK or T cell clones was not a feasible approach for studying its function. In order to determine whether FCRL6 inhibits NK cell–mediated killing of HLA-DR–expressing tumor cells, the NK-92 human cytotoxic NK cell line, which does not endogenously express FCRL6 on its surface, was transduced with either *FCRL6* or a vector control (Figure 8A). In addition, K562 target cells were transduced either with plasmids harboring the HLA-DRα and -DRβ1 subunits or with *CIITA* to drive endogenous MHC class II expression in these cells. K562 HLA-DRα+β1 and CIITA transductants, but not parental K562 cells or control transductants, expressed surface HLA-DR, by flow cytometric analysis (Figure 8A). K562 cells
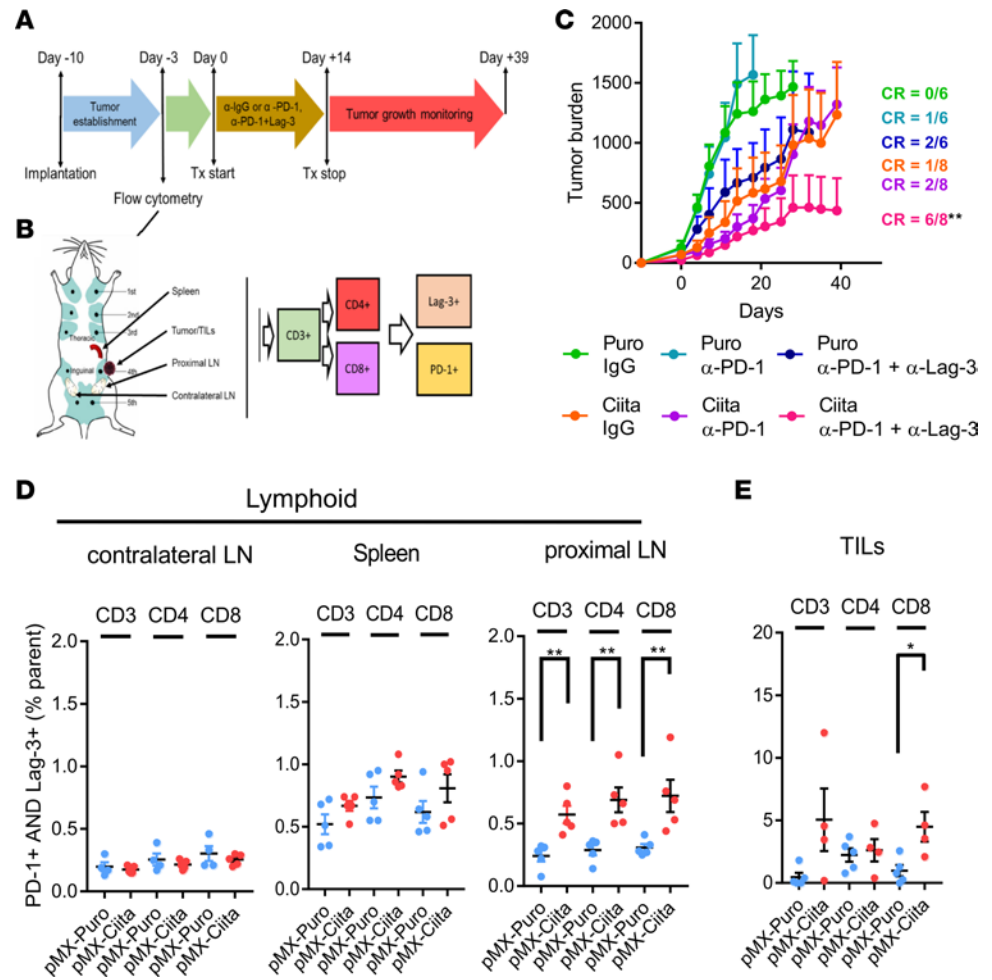
Figure 7. Combinatorial activity of PD-1– and Lag-3–neutralizing antibodies in MHC-II+ tumors. (**A**) Schematic of experimental strategy. On day –10, 1×10^6 MMTV-neu cells transduced with pMX-puro or pMX-Ciita were implanted by orthotopic injection in the 4th mammary fat pad of wild-type *FVB/n* mice. Seven days later, a subset of mice were sacrificed for flow cytometry analysis. On day 0, therapy was initiated consisting of twice weekly i.p. injections of anti-IgG control, anti–PD-1, or anti–PD-1+anti–Lag-3, which continued for 2 weeks. Tumors were monitored for growth over the next 39 days. (**B**) Schematic for analyzing tumor and lymphoid compartments by flow cytometry. (**C**) Tumor growth curves for treated mice. CR, complete response. **$P < 0.05$, χ^2 test across treatment groups in Ciita-expressing tumors. (**D**) Flow cytometry analysis of PD-1+/Lag-3+ lymphocytes by total CD3+ compartment or by CD3+/CD4+ or CD3+ CD8+ compartments in lymphoid tissues at 7 days after injection. **$P < 0.01$, 2-tailed Mann Whitney U test. (**E**) Flow cytometry analysis of PD-1+/Lag-3+ lymphocytes in tumors (TILs). *$P < 0.05$, Mann Whitney U test.

lack endogenous MHC-I expression and are therefore targeted by NK cell–mediated cytotoxicity. Thus, FCRL6+ NK-92 lines were assayed for their ability to kill K562 transductants (MHC-II+ and MHC-II–) in ^{51}Cr release experiments. These studies found that FCRL6+ NK-92 cells were significantly impaired in their capacity to lyse K562 DRαβ1- or CIITA-expressing targets but not control K562 cells (Figure 8A). Hence, FCRL6 is an inhibitory NK receptor for HLA-DR. Due to lack of a functional homolog in mice, only human systems are equipped to demonstrate this.

Since mouse FCRL6 differs structurally and functionally from its human relative (32), it is not a viable interspecies translational model for study. To test the hypothesis that the FCRL6/HLA-DR interaction might also inhibit CD8+ T cell responses, we examined the effect of FCRL6 blockade during pathogen-specific peptide stimulation in vitro. This analysis employed an anti-FCRL6 mAb (1D8) that is capable of blocking FCRL6 activation in coculture assays and obstructing FCRL6-Fc binding to HLA-DR transductants (27). Blood mononuclear cells from healthy donors were stimulated with pooled antigenic MHC class I–restricted peptides from CMV, EBV, and influenza virus epitopes (CEF peptide pool) in the presence of anti-FCRL6 or anti–PD-L1 (a positive control). Following a 6-day culture period, cells were collected,
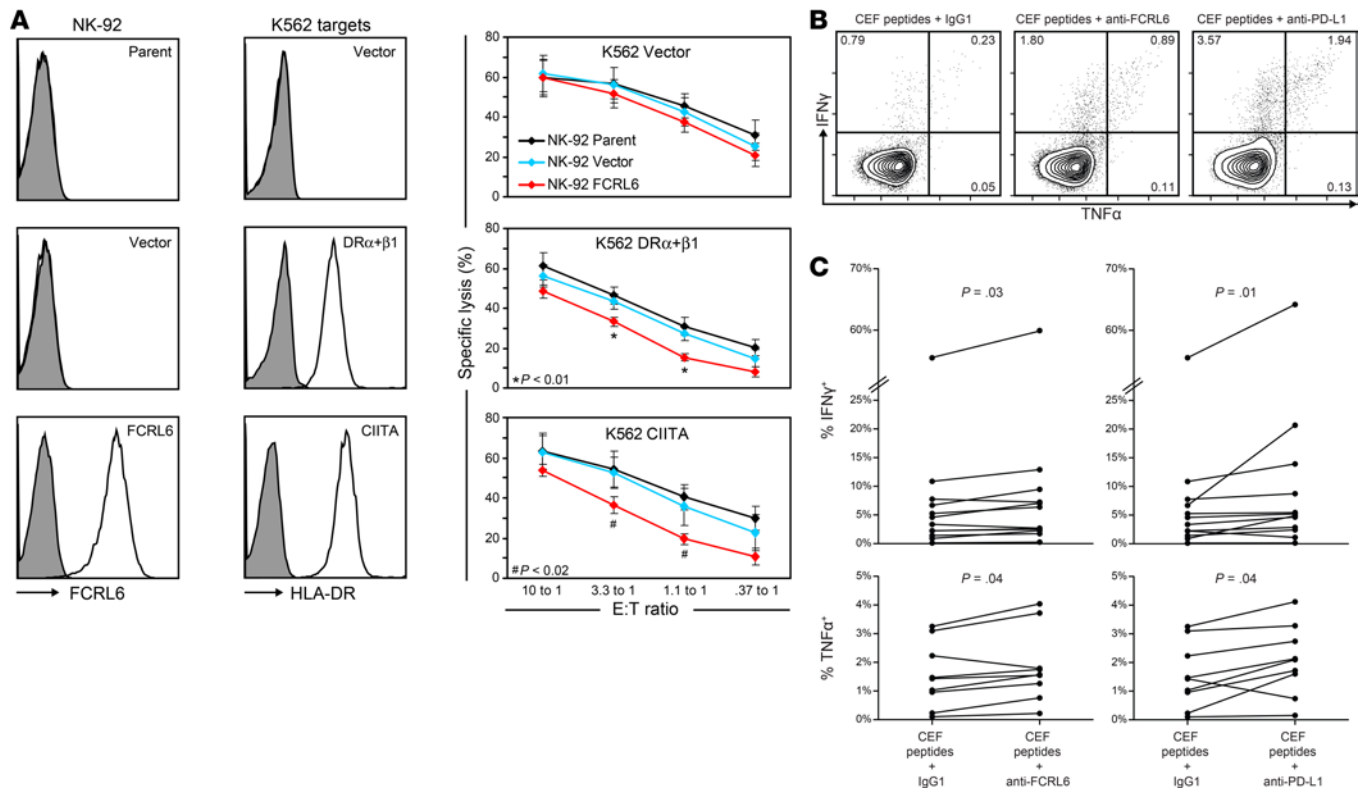
Figure 8. The alternative MHC-II receptor FCRL6 is an inhibitor of T cell and NK cell activity. (**A**) NK-92 and K562 transductants were stained with anti-FCRL6 or anti–HLA-DR, respectively. K562 vector (top), K562 DRa+b1 (middle), or K562 CIITA (bottom) transductants were cultured with NK-92 FCRL6 transductants (red lines), NK-92 vector (blue lines), or parental NK-92 cells (black lines) at various effector-to-target (E/T) ratios and assayed for K562 cytotoxicity in ^{51}Cr release assays. Experiments were performed in triplicate; lines represent the mean ± SD. n = 4; P values were calculated using Student's t test. *P < 0.01, #P < 0.02. (**B**) Blood mononuclear cells were cultured for 6 days in the presence of the CEF peptide pool with anti-FCRL6, anti–PD-L1, or an isotype-matched control mAb. Cells were collected, restimulated with CEF for 6 hours, and analyzed for intracellular cytokine production by flow cytometry. CD8+ T cells from one representative donor were gated, and the percentages of cells staining positive for the indicated cytokines are shown in the quadrants of each dot plot. (**C**) Paired data points from healthy donors (n = 12 for IFN-γ; n = 9 for TNF-α) are indicated by lines, and statistical significance was determined using the Wilcoxon signed-rank test.

restimulated with CEF, and assayed for cytokine production by intracellular staining. A significantly higher frequency of CD8+ T cells produced IFN-γ and TNF-α when cultured with the FCRL6 or PD-L1 mAbs compared with controls (Figure 8, B and C). Thus, these experiments identify the MHC-II receptor FCRL6 as a potential immunotherapeutic target and suppressor of NK and effector T cell activity.

Surprisingly, we found that *FCRL6*, but not its relative *FCRL3*, was significantly more highly expressed in MHC-II melanoma and lung cancers (Figure 9A), and the degree of *LAG3* and *FCRL6* showed a linear relationship with the fraction of HLA-DR+ tumor cells (R^2 = 0.65 and 0.45, respectively; Supplemental Figure 13). Furthermore, FCRL6 was elevated at relapse after progression on PD-1–targeted therapy both at the mRNA (Figure 9B) and at the protein level (Figure 9C and Supplemental Figure 14). In TNBC specimens, FCRL6+ lymphocytes were associated with tumor HLA-DR status (Figure 9D) and Lag-3 status (Figure 9E) but not MHC-I status (HLA-A; Supplemental Figure 15). Furthermore, concurrent presence of Lag-3+ lymphocytes and FCRL6+ lymphocytes was strikingly associated with high tumor-specific HLA-DR expression (Figure 9F). In healthy human subject PBMCs, activation of T cells by ligation of CD3/CD28 induced PD-1 and LAG3 expression over 24–72 hours but paradoxically and drastically reduced FCRL6 expression (Supplemental Figure 16A); however, between 24 and 72 hours, a rare but reproducible population of FCRL6+/LAG3+ cells was expanded in the CD8 compartment. In contrast, we did not detect an overlap in the expression of PD-1 and LAG3 by T cells, suggesting a potential biological implication of coexpression of FCRL6 and LAG3, which both bind MHC-II (Supplemental Figure 16B). Finally, among all breast tumors assessed, the presence of FCRL6 or Lag-3+ lymphocytes was associated with fewer cytotoxic CD8+ T cells (as defined by granzyme B+/CD8+ cells), supporting a hypothesis of active immune suppression mediated by these checkpoints (Figure 9G), particularly in MHC-II+ tumors. Importantly, neither Lag-3 nor FCRL6 colocalized to known immunosuppressive T regulatory cells by
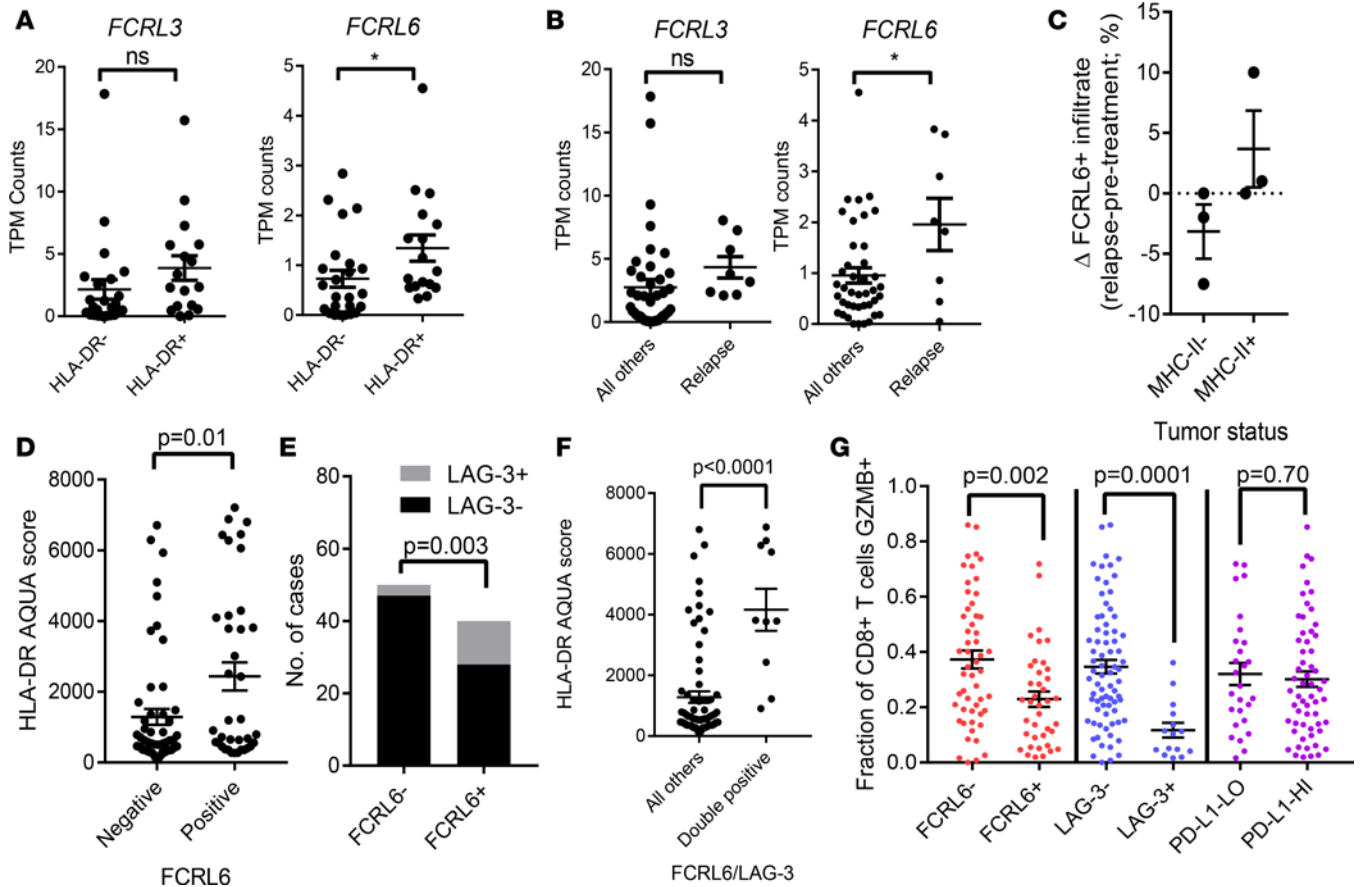
Figure 9. The alternative MHC-II receptor FCRL6 is enriched in MHC-II⁺ tumors and is associated with acquired resistance to anti–PD-1. (A) mRNA expression from RNA-sequencing data for *FCRL3* and *FCRL6* in MHC-II⁺ and MHC-II⁻ melanoma and lung cancers. (B) mRNA expression from RNA-sequencing data for *FCRL3* and *FCRL6* in untreated and postprogression/relapse specimens. (C) Quantification of IHC for FCRL6⁺ TILs in pairs of melanomas before and after resistance to anti–PD-1 therapy. (D) MHC-II/HLA-DR AQUA scores in triple-negative breast cancers stratified by the presence or absence of FCRL6⁺ lymphocytes. (E) Coexpression of Lag-3 and FCRL6 on TILs in postneoadjuvant triple-negative breast cancers. (F) MHC-II/HLA-DR AQUA scores in triple-negative breast cancers stratified by the presence or absence of FCRL6⁺ lymphocytes and Lag-3⁺ lymphocytes. (G) Fraction of CD8⁺ lymphocytes expressing granzyme B (AQUA), stratified by the presence or absence of FCRL6⁺ lymphocytes (IHC), Lag-3⁺ lymphocytes (IHC), or total tumor microenvironment PD-L1 expression (AQUA). *$P < 0.05$ by Mann Whitney U test.

dual Foxp3/MHC-II receptor IHC analysis in human melanomas (Supplemental Figure 17). Collectively, these data suggest that, like LAG-3, FCRL6 may be a novel inhibitory MHC-II receptor that is engaged preferentially in MHC-II⁺ tumors and may be partially responsible for adaptive resistance to anti–PD-1 therapy (Figure 10).

Discussion

Although anti–PD-1–based therapy may produce durable antitumor immune responses in some patients, a complex landscape of both intrinsic and acquired therapeutic resistance is emerging. Here, we report that MHC-II expression characterizes a particularly T cell–inflamed and immune-responsive subset of solid tumors. We further observed that this tumor-autonomous phenotype drives specific, context-dependent immune escape mechanisms involving alternative ligands to MHC-II, specifically LAG-3 and FCRL6.

In part, these data reinforce the growing awareness of the importance of MHC-II/CD4 interactions and shed light on how tumor-specific antigen presentation via MHC-II plays a role in modifying antitumor immunity via unconventional CD8-mediated suppression. Preclinical data demonstrate that in addition to promoting CD4⁺ Th1 differentiation in the tumor milieu, antigen-specific cytotoxic CD4⁺ T cells can also be generated (21, 22, 24, 33). Tumors with active class II–restricted antigen presentation via autonomous MHC-II expression likely generate these responses, contributing to antitumor immunity and subsequent reliance on peripheral tolerance mechanisms such as PD-1/L1 to maintain equilibrium. It is important to note that this study did not directly delineate the mechanism whereby expression of MHC-II on tumor cells recruits or activates CD4 cells.
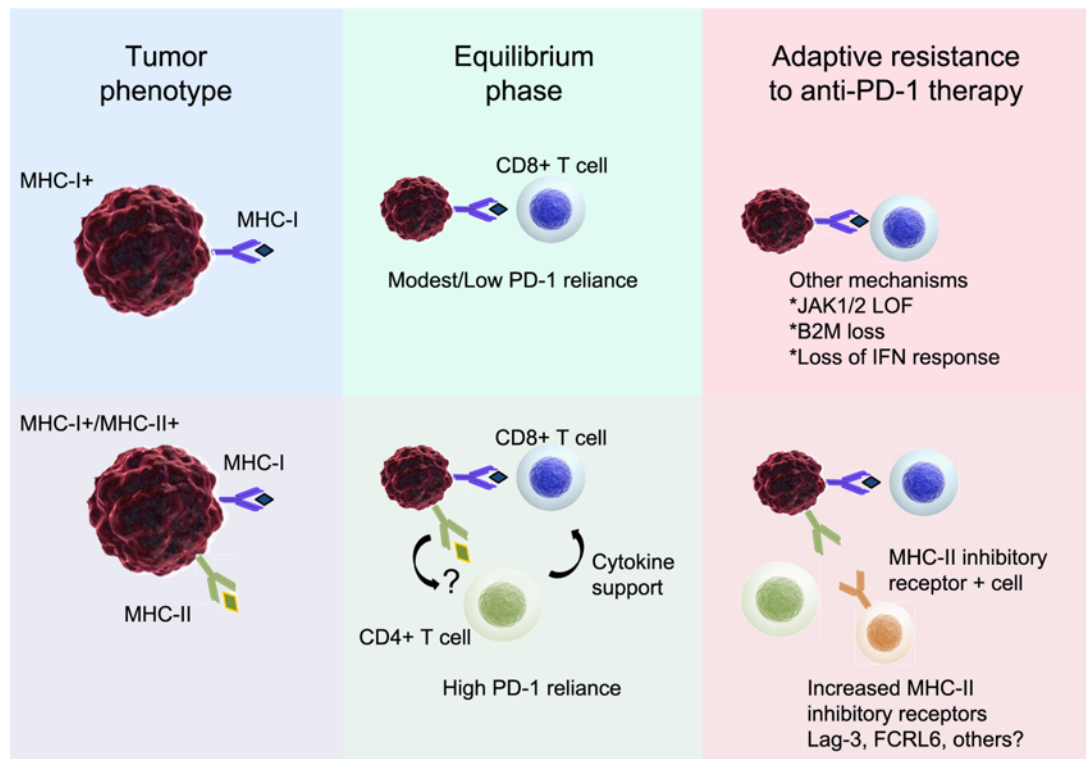
Figure 10. Proposed mechanism for selective adaptive resistance to anti–PD-1–targeted immunotherapy in MHC-II⁺ tumors.

Although published literature suggests that MHC-II⁺ tumor cells can indeed promote direct CD4⁺ Th cell activation and cytotoxicity (reviewed in ref. 34), based on our current results it is unclear whether this is a direct result of tumor-specific class II–restricted antigen presentation. A number of studies have demonstrated direct MHC-II⁺ tumor cell–mediated CD4⁺ T cell responses (33, 35, 36) and possibly even autonomous antigen expression through nonclassical class II antigen-processing pathways (37), but whether this plays a role in the enhanced antitumor immunity observed in MHC-II⁺ human tumors is still an enigma.

Nonetheless, our findings demonstrating a class II–targeting mechanism of acquired resistance to PD-1 therapy preferentially occurring in MHC-II⁺ tumors (i.e., upregulation of the inhibitory MHC-II receptors, LAG-3 and FCRL6) provide support for the in vivo and clinical importance of tumor-specific class II expression. Finally, upregulation of inflammation site licensing T cell chemokines in MHC-II⁺ tumors, downstream of CIITA activity, represents an intriguing additional mechanism whereby CIITA-mediated class II expression may recruit T cells to the tumor microenvironment.

Adaptive resistance to anti–PD-1 is an increasingly recognized clinical problem. While some responses appear remarkably durable, >50% of responding patients ultimately experience disease progression. The clinical management of these patients remains problematic, although some individuals may experience excellent clinical outcomes, with anti–PD-1 reinduction or management of isolated relapses (38). Effective combinatorial strategies are thus urgently needed, and our data suggest specific therapeutic approaches for MHC-II⁺ tumors.

Finally, our data suggest that molecular profiling at resistance may uncover therapeutic strategies uniquely suited for particular tumor subsets. This may provide a more rational approach than the current landscape of clinical trials that tests anti–PD-1–based combinations in patients who progress following monotherapy. In particular, we suggest that PD-1/PD-L1 and LAG-3 blockade may provide particular benefit for MHC-II–expressing tumors. Consistent with our translational data, this combination has already demonstrated early signs of clinical activity, particularly in patients with acquired resistance to anti–PD-1 (39).

In conclusion, our data suggest that MHC-II positivity on tumor cells provides selective pressure for LAG-3⁺ and FCRL6⁺ TILs to suppress MHC-II–mediated antigen presentation. Thus, the MHC-II⁺ phenotype may direct a specific pathway of adaptive resistance to PD-1–targeted immunotherapy. Finally, MHC-II⁺ tumor expression may be enriched in patients likely to respond to combination PD-1 and LAG-3 or possibly FCRL6 blockade.

Methods

Patient samples. For melanoma/lung cohorts, 58 patient samples and data were procured based on availability of tissue and were not collected according to a prespecified power analysis. These samples included 48 melanoma samples and 10 lung cancer samples. Included in these 58 samples were 8 relapse specimens (50 baseline pre–anti–PD-1 therapy), of which 5 were matched to a pre–anti–PD-1 therapy sample. Of these, 3 pairs were successfully RNA sequenced, 5 pairs were successfully scored for LAG-3 IHC, and 4 had sufficient tissue for FCRL6 IHC.

Tumor samples for the TMA and for the HLA-DR staining cohort were obtained from tumor biopsies or tumor resections obtained for clinical purposes. Samples were obtained within 2 years of start of anti–PD-1/PD-L1 therapy (nivolumab, pembrolizumab, atezolizumab). Only patients with available tumor samples and evaluable responses were included. In cases where multiple tissues were available for the same patient, the evaluable sample collected closest to PD-1 therapy was utilized for scoring. Clinical characteristics and objective response data were obtained by retrospective review of the electronic medical record. All responses were investigator-assessed, RECIST-defined responses or (in a single case) prolonged stable disease, with clinical benefit lasting >3 years.

For the TNBC cohort, 112 surgically resected tumor samples were from patients with TNBC diagnosed and treated with neoadjuvant chemotherapy at the Instituto Nacional de Enfermedades Neoplásicas in Lima, Perú. Clinical and pathological data were retrieved from medical records under an institutionally approved protocol (Instituto Nacional de Enfermedades Neoplásicas; INEN 10-018). Tumors were determined as triple negative if they were negative for estrogen receptor, progesterone receptor, and HER2 overexpression, as measured by IHC. The analysis of these samples has been previously described (20, 40, 41).

IHC and immunofluorescence. For dual IHC with HLA-DR (Santa Cruz, sc-53319; 1:1000), SOX10 (Cell Marque, 383A-74; 1:100), FoxP3 (Cell Signaling Technology, 98377; 1:100), and FCRL6 (clone 7B7; 1:100) (42), tumor sections were stained overnight at 4°C with both antibodies (HLA-DR plus SOX10 or FCRL6 plus FoxP3 dual IHC). Antigen retrieval was performed using citrate buffer (pH 6) using a Biocare Decloaking Chamber. The visualization system utilized was MACH2 Stain 2 (Biocare) using DAB (Dako) and Warp Red (Biocare), and counterstained with hematoxylin. For FoxP3 (Invitrogen, 14-4777-82; 1:100) and Lag3 (Cell Signaling Technology, 15372; 1:200), tumor sections were stained overnight at 4°C with both antibodies. Antigen retrieval was performed using citrate buffer (pH6) using a Biocare Decloaking Chamber. The visualization system utilized was MACH2 Stain 1 (Biocare) using DAB (Dako) and Warp Red (Biocare), and counterstained with hematoxylin. HLA-DR scoring in the tumor compartment was performed as described previously (12). For single IHC analysis of FCRL6 (clone 7B7; 1:100) and LAG-3 (Cell Signaling Technology, 15372; 1:200) detection, a citrate buffer (pH 6) was used for antigen retrieval using a Biocare Decloaking Chamber, with Envision for the visualization system. For CD4 and CD8 staining, slides were placed on a Leica Bond Max IHC stainer. All steps besides dehydration, clearing, and coverslipping were performed on the Bond Max. Heat-induced antigen retrieval was performed on the Bond Max using their Epitope Retrieval 2 solution for 20 minutes. Slides were incubated with anti-CD4 (PA0427, Leica) or anti-CD8 (MS-457-R7, Thermo Scientific) for 1 hour. The Bond Polymer Refine detection system was used for visualization. CD4 and CD8 were scored as the percentage of infiltrating CD4$^+$ or CD8$^+$ cells in the tumor area. HLA-DR immunofluorescence/AQUA and PD-L1 immunofluorescence/AQUA were performed as previously described (19, 41, 43). Additional multiplexed IHC was performed with sequential staining for CD4 (M7310, 1:50, DAKO), CD8 (M7103, 1:400, DAKO), and granzyme B (GrB-7, 1:300, DAKO); amplified with EnVision+HRP Mouse (DAKO); and detected with TSA-Cy5 (1:50, Perkin Elmer), Opal 540 (1:200, Perkin Elmer), and Opal 620 (1:200, Perkin Elmer), respectively. Additionally, staining included pan-cytokeratin (Z0622, 1:200, DAKO) detected with goat anti-rabbit Alexa Fluor 488 (1:200, Life Technologies), and DAPI. Digital imaging was performed on the Vectra 2 (Perkin Elmer), and expression of all CD4$^+$ and CD8$^+$ cells and the percentage of CD4$^+$ or CD8$^+$ cells also expressing granzyme B was quantified using AQUA Technology (Navigate BioPharma Services Inc.). Dual ISH-IHC was performed following the Advanced Cell Diagnostics pretreatment protocol for FFPE tissue. Target retrieval time followed a 30-minute incubation at 99°C and incubation with Protease Plus (Advanced Cell Diagnostics) for 30 minutes at 40°C. After this, we used the RNAscope BaseScope kit (Advanced Cell Diagnostics, catalog 322910) with the CIITA probe (Advanced Cell Diagnostics, catalog 418721) to step 6 and then HLA-DR (Santa Cruz, sc-53319; 1:1000). Overnight

incubation was performed at 4°C with Envision as the visualization system and DAB as the first chromogen applied for 5 minutes. We then used Fast Red dye (Advanced Cell Diagnostics) for 10 minutes, counterstained with hematoxylin using ammonia water as the bluing solution, dried at 60°C for 20 minutes, and mounted with VectaMount (Vector Laboratories).

TCGA data analysis. TCGA data were accessed through the cBio data portal (43) or through TCGA data portal for processed RNA-SEQ data analysis (44).

Cell culture. MMTV-neu cells were isolated from primary mammary tumor cells growing in transgenic *FVB/N* mice and passaged serially for >10 passages in DMEM/F12 media supplemented with 10% FBS, 20 ng/ml EGF, 500 ng/ml hydrocortisone, and 10 ng/ml insulin to generate an established cell line. The presence of rat neu (Western blot) in the cells is diagnostic for the authenticity of the cells and is performed on a regular basis. K562 cells were obtained from ATCC and maintained in Iscove's DMEM supplemented with 10% FCS, 100 units/ml penicillin and streptomycin, and 50 μM β-mercaptoethanol. NK-92 cells were obtained from ATCC and maintained according to the manufacturer's recommendations.

Lentiviral/retroviral transduction. The murine Ciita open reading frame was obtained from Genecopoeia, amplified by PCR with restriction sites, and cloned into the pMX-puro multiple cloning site. Retroviral production was performed in Amphopak cells. MMTV-neu cells were transduced as previously described (40).

For NK-92 cell line transduction, an FCRL6 lentiviral vector (pEF.FCRL6) was generated by replacing the *GFP* gene in pEF.GFP (45) with the full-length *FCRL6* cDNA. pEF.FCRL6 and pEF.GFP lentiviruses were packaged in 293T cells for transduction, and stable transductants were FACS sorted for FCRL6 or GFP enrichment. *HLA-DRα* (DRA*0101), *HLA-DRβ1* (DRB1*040101), and *CIITA* were subcloned into the pMX-PIE retroviral vector, which contains the *GFP* gene downstream of an internal ribosomal entry site (IRES) and used to transduce K562 cells as described previously (46). Prior to retroviral transduction, K562 cells were transiently transfected with the murine ecotropic receptor MCAT1 (a gift of Gotz Ehrhardt, University of Toronto, Toronto, Ontario, Canada) by electroporation. Doubly transduced HLA-DRαβ+1 cells were sorted for GFP expression and surface staining with the PE-labeled HK14 anti–HLA-DR mAb (MilliporeSigma); singly transduced HLA-DRα, HLA-DRβ1, and CIITA cells were FACS sorted for GFP.

Mouse studies. MMTV-neu cells (1×10^6 cells) were injected in the 4th mammary fat pad of syngeneic *FVB/N* mice. Following tumor establishment, when palpable tumors reached 100 mm^3, mice were observed for tumor growth rate, spontaneous rejection, or, in later studies, randomized to treatment groups or vehicle control. Murine α–PD-1 and α–Lag-3 blocking antibodies were purchased from BioXcell and injected i.p. twice weekly at 100 μg/100 μl for a total of 2 weeks. Control IgG was also administered i.p. in vehicle-treated mice. Mice were monitored twice weekly for tumor formation and tumor burden (digital calipers) using the formula (length/$2 \times$ width^2).

NanoString analysis. NanoString analysis was performed on mouse tumors using the mouse Pan-Cancer Immunology panel as previously described (20, 40). Briefly, single cross sections of FFPE tumors harvested at the humane endpoint (2 cm^2 total tumor burden) were used for RNA preparation using the Maxwell-16 FFPE RNA kit (Promega), and 50 ng total RNA >300 nt was used for input into nCounter hybridizations. QC measures and normalization of data were performed using the nSolver analysis package and R.

Flow cytometry. Flow cytometry was performed on an Attune NxT Flow Cytometer (Thermo Fisher). For basic mouse immunophenotyping, freshly dissociated tumors were stained with viability dye (Zombie Violet; Biolegend) and fluorophore-conjugated anti-CD3 (17A2; A488), anti-CD4 (GK1.5; APC), anti-CD8 (53-6.7; PE-Cy7), anti–PD-1 (29F.1A12; BV711), and anti–Lag-3 (C9B7W; PE) (all from Biolegend). Additional antibodies utilized were anti-IA/IE (MHC-II; M5/114.15.2; A488) and anti-CD45 (30-F11; A700) (both from Biolegend). For human lymphocyte immunophenotyping, freshly isolated peripheral blood mononuclear cells were stained with viability dye (Zombie Aqua; Biolegend) and fluorophore-conjugated anti-CD3 (HIT3a; AF488), anti-CD4 (OKT4; APC/Cy7), anti-CD8 (HIT89a; PE), and anti–PD-1 (EH12.2H7; PE/Cy7) (all from Biolegend). Additional antibodies utilized were anti-FCRL6 (7B7, in-house) and anti-Lag3 (3DS223H; SB436, eBiosciences). All antibodies were titrated to optimal concentrations prior to staining.

Mass cytometry. Thawed samples of previously processed and cryopreserved melanoma tumors and healthy PBMCs were washed and treated with Cell-ID Cisplatin and diluted to 5 μM final concentration for viability staining per the manufacturer's instructions (Fluidigm Sciences) (47). After incubation with viability reagent, cells were washed in PBS containing 1% BSA (Cell Staining Media [CSM]). A master mix of surface panel antibodies (Supplemental Table 1) was added to each sample for a final staining volume of 50 μl and incubated at room temperature for 30 minutes. Cells were then washed twice with CSM and

fixed with a final concentration of 1.6% paraformaldehyde (PFA, Electron Microscopy Sciences). Cells were then washed twice, first with CSM and then with PBS, and then permeabilized in –20°C methanol and incubated overnight at –20°C. After washing once in PBS and once in CSM, a master mix of postpermeabilization panel antibodies (Supplemental Table 1) was added to each sample at a desired concentration for a final staining volume of 50 μl and incubated at room temperature for 30 minutes. Cell were then washed in PBS and stained with the Cell-ID iridium DNA intercalator (Fluidigm Sciences) and 1.6% PFA. Subsequently, cells were washed in MilliQ water (MilliporeSigma) and suspended in EQ beads (Fluidigm) and water solution. Stained samples were collected at the Vanderbilt University Mass Cytometry Center of Excellence on a Helios mass cytometer (Fluidigm Sciences). All events were normalized prior to analysis using EQ normalization beads (Fluidigm). Mass cytometry data (.fcs files) were evaluated with biaxial gating as well as viSNE on Cytobank's cloud-based user interface (48–50).

Custom conjugated antibodies were obtained purified, carrier free from the listed provider and labeled with the listed metal (Supplemental Table 1) using the protocol provided by Fluidigm.

RNA sequencing. Total RNA quality was assessed using the 2200 Tapestation (Agilent). At least 20 ng DNase-treated total RNA, with at least 30% of the RNA fragments with a size >200 nt, was used to generate RNA Access libraries (Illumina) following the manufacturer's recommendations. Library quality was assessed using the 2100 Bioanalyzer (Agilent), and libraries were quantitated using KAPA Library Quantification Kits (KAPA Biosystems). Pooled libraries were subjected to 75-bp paired-end sequencing according to the manufacturer's protocol (Illumina HiSeq3000). Bcl2fastq2 Conversion Software (Illumina) was used to generate demultiplexed Fastq files.

QC for the paired-end raw sequencing reads of all samples was performed using FastQC (51) for the analysis of sequence quality, GC content, the presence of adaptors, overrepresented *k*-mers, and duplicated reads. Sequencing reads were mapped to human reference genome GRCH38 (release-85, Ensembl, ref. 52) using STAR 2.2.1 with 2-pass mapping (53, 54). QC for read alignment and mapping was evaluated with RSeQC (55) for sequencing saturation, mapped read clipping profile, mapped read distribution, and coverage uniformity. The transcripts per million (TPM) values were calculated using RSEM (56) and used to assess the global quality and reproducibility of the RNA-sequencing data set and exported for downstream data analyses.

Chromium-51 release assays. ^{51}Cr release experiments were performed as described previously (57). Briefly, 1×10^6 K562 transductants were labeled for 1 hour with 100 μCi/ml ^{51}Cr (Perkin Elmer), washed, and plated at 1×10^4 cells/well in 96-well round-bottom plates. NK-92 cells were washed, resuspended in warm RPMI 1640 media containing 10% FCS, and plated with K562 cells at various effector to target ratios. Plates were spun at 1000 rpm for 1 minute and then cultured for 4 hour at 37°C. Supernatants were collected and transferred to 96-well scintillant-coated plates (Perkin Elmer), and ^{51}Cr activity was measured using a TopCount NXT instrument (Packard). Spontaneous release and total release were assessed from K562 cells cultured in media alone or 2% Triton X-100, respectively. Specific lysis was calculated as described previously (57). To equalize culture conditions, each NK-92 cell line was seeded in fresh media at a concentration of 2×10^5 cells/ml and cultured for 2 days prior to performing cytotoxicity experiments.

Healthy donor T cell assays. Freshly isolated PBMCs were cultured in RPMI 1640 media supplemented with 10% FCS, 100 units/ml penicillin and streptomycin, and 50 μM β-mercaptoethanol, and a CEF peptide pool (Anaspec) at 0.4 μg/ml. Control IgG1 (Southern Biotechnology Associates), anti–PD-L1 (eBioscience), and anti-FCRL6 (1D8) (27) mAbs were added at 5 μg/ml to the initial cultures, and on day 6, cells were collected, washed, and restimulated for 6 hours with CEF at 2 μg/ml in the presence of brefeldin-A and monensin (Biolegend). Cells were then stained for surface markers, fixed and permeabilized, cytoplasmically stained with anti–IFN-γ APC and anti–TNF-α PE (Biolegend), and analyzed with a Cyan flow cytometer.

Statistics. Statistics were performed as indicated using R or GraphPad Prism. $P < 0.05$ was considered statistically significant for all studies. For paired analysis, a 2-tailed paired *t* test was utilized. Log-transformed data were utilized prior to analysis, where distributions demonstrated heteroscedasticity in linear form. For data with unequal variances, even after transformation, nonparametric equivalents were utilized. For multigroup comparisons, ANOVA was utilized with Tukey's post hoc analysis to identify group-specific differences. Where error bars are presented, all data are mean ± SEM.

Study approval. All patients provided informed written consent. All human samples were obtained in accordance with the Declaration of Helsinki following protocols approved by Vanderbilt University Medical Center Institutional Review Board (Vanderbilt IRB 030220 and 100178). All murine studies were performed under approval and in accordance with Vanderbilt IACUC-approved protocols.

Author contributions

MJN, DBJ, DMS, JMB, and RSD: acquisition of data, design of research studies, and analysis of experimental data. DYW, EC, DBJ, and LH: chart review, consent of patients, and analysis of clinical data. MVE, PIEG, VS, RS, and MES: assay optimization, acquisition, and analysis and interpretation of histology and pathology. CHC and PBF: conduct of CyTOF and flow data acquisition and interpretation. PTD and SRO: conduct of experiments and acquisition of data. DLR, JYK, and JB: analysis of immunofluorescence and AQUA data. JAS, RSD, JMB, DBJ, and SL: interpretation of experimental results and hypothesis design. YW and YX: statistical design and interpretation. All authors were involved in the interpretation of data and writing of the final manuscript.

Acknowledgments

Address correspondence to: Justin Balko, Vanderbilt University Medical Center, 2200 Pierce Avenue, 777 PRB, Nashville, Tennessee 37232-6307, USA. Phone: 615.322.4967; Email: justin.balko@vanderbilt.edu. Or to: Randall Davis, University of Alabama School of Medicine, 1720 2nd Avenue South, SHEL 413, Birmingham, Alabama 35294-2182, USA. Phone: 205.934.1816; Email: rsdavis@uab.edu.

1. Balar AV, Weber JS. PD-1 and PD-L1 antibodies in cancer: current status and future directions. *Cancer Immunol Immunother*. 2017;66(5):551–564.
2. Shin DS, et al. Primary resistance to PD-1 blockade mediated by JAK1/2 mutations. *Cancer Discov*. 2017;7(2):188–201.
3. Zaretsky JM, et al. Mutations associated with acquired resistance to PD-1 blockade in melanoma. *N Engl J Med*. 2016;375(9):819–829.
4. Koyama S, et al. Adaptive resistance to therapeutic PD-1 blockade is associated with upregulation of alternative immune checkpoints. *Nat Commun*. 2016;7:10501.
5. Lu YC, Robbins PF. Cancer immunotherapy targeting neoantigens. *Semin Immunol*. 2016;28(1):22–27.
6. Rizvi NA, et al. Cancer immunology. Mutational landscape determines sensitivity to PD-1 blockade in non-small cell lung cancer. *Science*. 2015;348(6230):124–128.
7. Schumacher TN, Schreiber RD. Neoantigens in cancer immunotherapy. *Science*. 2015;348(6230):69–74.
8. Snyder A, et al. Genetic basis for clinical response to CTLA-4 blockade in melanoma. *N Engl J Med*. 2014;371(23):2189–2199.
9. Van Allen EM, et al. Genomic correlates of response to CTLA-4 blockade in metastatic melanoma. *Science*. 2015;350(6257):207–211.
10. Zou W, Wolchok JD, Chen L. PD-L1 (B7-H1) and PD-1 pathway blockade for cancer therapy: mechanisms, response biomarkers, and combinations. *Sci Transl Med*. 2016;8(328):328rv4.
11. Hugo W, et al. Genomic and transcriptomic features of response to anti-PD-1 therapy in metastatic melanoma. *Cell*. 2016;165(1):35–44.
12. Johnson DB, et al. Melanoma-specific MHC-II expression represents a tumour-autonomous phenotype and predicts response to anti-PD-1/PD-L1 therapy. *Nat Commun*. 2016;7:10582.
13. Roemer MGM, et al. Major histocompatibility complex class II and programmed death ligand 1 expression predict outcome after programmed death 1 blockade in classic Hodgkin lymphoma. *J Clin Oncol*. 2018;36(10):942–950.
14. Rodig SJ, et al. MHC proteins confer differential sensitivity to CTLA-4 and PD-1 blockade in untreated metastatic melanoma. *Sci Transl Med*. 2018;10(450):eaar3342.
15. Johnson DB, et al. Quantitative spatial profiling of PD-1/PD-L1 interaction and HLA-DR/IDO-1 predicts improved outcomes of anti-PD-1 therapies in metastatic melanoma. *Clin Cancer Res*. 2018;24(21):5250–5260.
16. Haastert B, Mellanby RJ, Anderton SM, O'Connor RA. T cells at the site of autoimmune inflammation show increased potential for trogocytosis. *PLoS One*. 2013;8(12):e81404.
17. Baixeras E, et al. Characterization of the lymphocyte activation gene 3-encoded protein. A new ligand for human leukocyte antigen class II antigens. *J Exp Med*. 1992;176(2):327–337.
18. Huard B, Tournier M, Hercend T, Triebel F, Faure F. Lymphocyte-activation gene 3/major histocompatibility complex class II interaction modulates the antigenic response of CD4+ T lymphocytes. *Eur J Immunol*. 1994;24(12):3216–3221.
19. Ashizawa T, et al. Antitumor effect of programmed death-1 (PD-1) blockade in humanized the NOG-MHC double knockout mouse. *Clin Cancer Res*. 2017;23(1):149–158.
20. Loi S, et al. RAS/MAPK activation is associated with reduced tumor-infiltrating lymphocytes in triple-negative breast cancer: therapeutic cooperation between MEK and PD-1/PD-L1 immune checkpoint inhibitors. *Clin Cancer Res*. 2016;22(6):1499–1509.
21. Lee YS, Kim SH, Cho JA, Kim CW. Introduction of the CIITA gene into tumor cells produces exosomes with enhanced

anti-tumor effects. *Exp Mol Med*. 2011;43(5):281–290.

22. Meazza R, Comes A, Orengo AM, Ferrini S, Accolla RS. Tumor rejection by gene transfer of the MHC class II transactivator in murine mammary adenocarcinoma cells. *Eur J Immunol*. 2003;33(5):1183–1192.

23. Mortara L, et al. CIITA-induced MHC class II expression in mammary adenocarcinoma leads to a Th1 polarization of the tumor microenvironment, tumor rejection, and specific antitumor memory. *Clin Cancer Res*. 2006;12(11 Pt 1):3435–3443.

24. Yan H, et al. CD4+ T cell-mediated cytotoxicity eliminates primary tumor cells in metastatic melanoma through high MHC class II expression and can be enhanced by inhibitory receptor blockade. *Tumour Biol*. 2016;37(12):15949–15958.

25. Wong D, et al. Genomic mapping of the MHC transactivator CIITA using an integrated ChIP-seq and genetical genomics approach. *Genome Biol*. 2014;15(10):494.

26. Groom JR, Luster AD. CXCR3 in T cell function. *Exp Cell Res*. 2011;317(5):620–631.

27. Schreeder DM, Cannon JP, Wu J, Li R, Shakhmatov MA, Davis RS. Cutting edge: FcR-like 6 is an MHC class II receptor. *J Immunol*. 2010;185(1):23–27.

28. Wilson TJ, Presti RM, Tassi I, Overton ET, Cella M, Colonna M. FcRL6, a new ITIM-bearing receptor on cytolytic cells, is broadly expressed by lymphocytes following HIV-1 infection. *Blood*. 2007;109(9):3786–3793.

29. Schreeder DM, Pan J, Li FJ, Vivier E, Davis RS. FCRL6 distinguishes mature cytotoxic lymphocytes and is upregulated in patients with B-cell chronic lymphocytic leukemia. *Eur J Immunol*. 2008;38(11):3159–3166.

30. Jiang YZ, et al. Interaction of natural killer cells with MHC class II: reversal of HLA-DR1-mediated protection of K562 trans-fectant from natural killer cell-mediated cytolysis by brefeldin-A. *Immunology*. 1996;87(3):481–486.

31. Weichold FF, et al. Regulation of a graft-versus-leukemia effect by major histocompatibility complex class II molecules on leu-kemia cells: HLA-DR1 expression renders K562 cell tumors resistant to adoptively transferred lymphocytes in severe combined immunodeficiency mice/nonobese diabetic mice. *Blood*. 1997;90(11):4553–4558.

32. Davis RS. Fc receptor-like molecules. *Annu Rev Immunol*. 2007;25:525–560.

33. Thompson JA, Dissanayake SK, Ksander BR, Knutson KL, Disis ML, Ostrand-Rosenberg S. Tumor cells transduced with the MHC class II Transactivator and CD80 activate tumor-specific CD4+ T cells whether or not they are silenced for invariant chain. *Cancer Res*. 2006;66(2):1147–1154.

34. Haabeth OA, et al. How do CD4(+) T cells detect and eliminate tumor cells that either lack or express MHC class II molecules? *Front Immunol*. 2014;5:174.

35. Bou Nasser Eddine F, Forlani G, Lombardo L, Tedeschi A, Tosi G, Accolla RS. CIITA-driven MHC class II expressing tumor cells can efficiently prime naive CD4+ TH cells in vivo and vaccinate the host against parental MHC-II-negative tumor cells. *Oncoimmunology*. 2017;6(1):e1261777.

36. Guerry D, et al. HLA-DR histocompatibility leukocyte antigens permit cultured human melanoma cells from early but not advanced disease to stimulate autologous lymphocytes. *J Clin Invest*. 1984;73(1):267–271.

37. Matsuzaki J, et al. Nonclassical antigen-processing pathways are required for MHC class II-restricted direct tumor recognition by NY-ESO-1-specific CD4(+) T cells. *Cancer Immunol Res*. 2014;2(4):341–350.

38. Wang DY, et al. Clinical features of acquired resistance to anti-PD-1 therapy in advanced melanoma. *Cancer Immunol Res*. 2017;5(5):357–362.

39. Ascierto PA, et al. Initial efficacy of anti-lymphocyte activation gene-3 (anti–LAG-3; BMS-986016) in combination with nivolumab (nivo) in pts with melanoma (MEL) previously treated with anti–PD-1/PD-L1 therapy. *J Clin Oncol*. 2017;35(Suppl_15):9520.

40. Balko JM, et al. Molecular profiling of the residual disease of triple-negative breast cancers after neoadjuvant chemotherapy identifies actionable therapeutic targets. *Cancer Discov*. 2014;4(2):232–245.

41. Balko JM, et al. Triple-negative breast cancers with amplification of JAK2 at the 9p24 locus demonstrate JAK2-specific depen-dence. *Sci Transl Med*. 2016;8(334):334ra53.

42. Schreeder DM, Pan J, Li FJ, Vivier E, Davis RS. FCRL6 distinguishes mature cytotoxic lymphocytes and is upregulated in patients with B-cell chronic lymphocytic leukemia. *Eur J Immunol*. 2008;38(11):3159–3166.

43. Cerami E, et al. The cBio cancer genomics portal: an open platform for exploring multidimensional cancer genomics data. *Can-cer Discov*. 2012;2(5):401–404.

44. Cancer Genome Atlas Network. Comprehensive molecular portraits of human breast tumours. *Nature*. 2012;490(7418):61–70.

45. Zufferey R, et al. Self-inactivating lentivirus vector for safe and efficient in vivo gene delivery. *J Virol*. 1998;72(12):9873–9880.

46. Ehrhardt GR, Davis RS, Hsu JT, Leu CM, Ehrhardt A, Cooper MD. The inhibitory potential of Fc receptor homolog 4 on memory B cells. *Proc Natl Acad Sci USA*. 2003;100(23):13489–13494.

47. Fienberg HG, Simonds EF, Fantl WJ, Nolan GP, Bodenmiller B. A platinum-based covalent viability reagent for single-cell mass cytometry. *Cytometry A*. 2012;81(6):467–475.

48. Kotecha N, Krutzik PO, Irish JM. Web-based analysis and publication of flow cytometry experiments. *Curr Protoc Cytom*. 2010;Chapter 10:Unit10.17.

49. Amir el-AD, et al. viSNE enables visualization of high dimensional single-cell data and reveals phenotypic heterogeneity of leukemia. *Nat Biotechnol*. 2013;31(6):545–552.

50. Bruggner RV, Bodenmiller B, Dill DL, Tibshirani RJ, Nolan GP. Automated identification of stratifying signatures in cellular subpopulations. *Proc Natl Acad Sci USA*. 2014;111(26):E2770–E2777.

51. Andrew S. Babraham Institute. FastQC: a quality control tool for high throughput sequence data. https://www.bioinformatics.babraham.ac.uk/projects/fastqc/. Accessed November 15, 2018.

52. Aken BL, et al. The Ensembl gene annotation system. *Database (Oxford)*. 2016;2016:baw093.

53. Dobin A, et al. STAR: ultrafast universal RNA-seq aligner. *Bioinformatics*. 2013;29(1):15–21.

54. Dobin A, Gingeras TR. Mapping RNA-seq reads with STAR. *Curr Protoc Bioinformatics*. 2015;51:11.14.1–11.1419.

55. Wang L, Wang S, Li W. RSeQC: quality control of RNA-seq experiments. *Bioinformatics*. 2012;28(16):2184–2185.

56. Li B, Dewey CN. RSEM: accurate transcript quantification from RNA-Seq data with or without a reference genome. *BMC Bio-informatics*. 2011;12:323.

57. Whiteside TL. Measurement of cytotoxic activity of NK/LAK cells. *Curr Protoc Immunol*. 2001;Chapter 7:Unit 7.18.